

High-resolution infrared spectroscopy of $^{14}\text{N}^{15}\text{N}^{16}\text{O}$ and $^{15}\text{N}^{14}\text{N}^{16}\text{O}$ in the 1200–3500 cm^{−1} region

C.Y. Wang^a, A.W. Liu^{a,*}, V.I. Perevalov^b, S.A. Tashkun^b, K.F. Song^a, S.M. Hu^a

^aHefei National Laboratory for Physical Sciences at the Microscale, University of Science and Technology of China, Hefei 230026, China

^bLaboratory of Theoretical Spectroscopy, Institute of Atmospheric Optics, SB, Russian Academy of Science, 1, Akademichekii av., 634055 Tomsk, Russia

ARTICLE INFO

Article history:

Received 20 April 2009

In revised form 22 June 2009

Available online 1 July 2009

Keywords:

Nitrous oxide

Infrared

Fourier-transform spectroscopy

Line position

Spectroscopic parameters

ABSTRACT

We present a continuation of our investigation of the second most abundant isotopic species of nitrous oxide, $^{14}\text{N}^{15}\text{N}^{16}\text{O}$ and $^{15}\text{N}^{14}\text{N}^{16}\text{O}$, in the infrared (IR). Our two previous contributions looked at the 3500–9000 cm^{−1} region for $^{14}\text{N}^{15}\text{N}^{16}\text{O}$ and $^{15}\text{N}^{14}\text{N}^{16}\text{O}$, respectively, in the 3500–9000 cm^{−1} region. The use of highly enriched isotopologue samples in this study allowed us to go further into the IR, down to 1200 cm^{−1}. A total of 22742 transitions have been assigned based on the effective Hamiltonian model, with 108 of them being reported here for the first time. Rovibrational analyses of 98, 101, 8, 3, 6, 1 and 1 bands for the $^{14}\text{N}^{15}\text{N}^{16}\text{O}$, $^{15}\text{N}^{14}\text{N}^{16}\text{O}$, $^{15}\text{N}^{15}\text{N}^{16}\text{O}$, $^{14}\text{N}^{15}\text{N}^{18}\text{O}$, $^{15}\text{N}^{14}\text{N}^{18}\text{O}$, $^{14}\text{N}^{15}\text{N}^{17}\text{O}$ and $^{15}\text{N}^{14}\text{N}^{17}\text{O}$ isotopologues, respectively, were also performed.

© 2009 Elsevier Inc. All rights reserved.

1. Introduction

In the recent contributions [1,2], we presented rovibrational analysis of the high-resolution Fourier-transform spectrum of the second most abundant isotopic species of nitrous oxide, $^{14}\text{N}^{15}\text{N}^{16}\text{O}$ and $^{15}\text{N}^{14}\text{N}^{16}\text{O}$, in the 3500–9000 cm^{−1} region. In this work, we will extend the high-resolution spectroscopic study down to 1200 cm^{−1}, where lots of hot bands are located.

A review of the previous spectroscopic work on $^{14}\text{N}^{15}\text{N}^{16}\text{O}$ and $^{15}\text{N}^{14}\text{N}^{16}\text{O}$ spectra was described in [1,2], so we will not repeat it here. The present work is devoted to generating a complete list of the line positions of $^{14}\text{N}^{15}\text{N}^{16}\text{O}$ and $^{15}\text{N}^{14}\text{N}^{16}\text{O}$ molecules in the 1200–3500 cm^{−1} region. The determination of experimental line intensity and the global modeling will be discussed in our subsequent paper. Altogether, 22742 transitions due to 98, 101, 8, 3, 6, 1 and 1 bands for the $^{14}\text{N}^{15}\text{N}^{16}\text{O}$, $^{15}\text{N}^{14}\text{N}^{16}\text{O}$, $^{15}\text{N}^{15}\text{N}^{16}\text{O}$, $^{14}\text{N}^{15}\text{N}^{18}\text{O}$, $^{15}\text{N}^{14}\text{N}^{18}\text{O}$, $^{14}\text{N}^{15}\text{N}^{17}\text{O}$ and $^{15}\text{N}^{14}\text{N}^{17}\text{O}$ isotopologues, respectively, were identified in the 1200–3500 cm^{−1} region. (Note that the HITRAN [3] notation will be used throughout the paper, for the seven isotopologues contributing to the spectrum: $^{14}\text{N}^{15}\text{N}^{16}\text{O}$: 456, $^{15}\text{N}^{14}\text{N}^{16}\text{O}$: 546, $^{15}\text{N}^{15}\text{N}^{16}\text{O}$: 556, $^{14}\text{N}^{15}\text{N}^{18}\text{O}$: 458, $^{15}\text{N}^{14}\text{N}^{18}\text{O}$: 548, $^{14}\text{N}^{15}\text{N}^{17}\text{O}$: 457, and $^{15}\text{N}^{14}\text{N}^{17}\text{O}$: 547). This study newly reports 108 of these 218 bands; the others 110 others are significantly extended and improved.

The paper is organized as following: in Section 2, we present briefly the experimental conditions employed to measure the spec-

tra. In Section 3, the vibrational assignments and a band-by-band rotational analysis are presented. The results will be discussed in Section 4.

2. Experiment

Two samples of 456 and 546 enriched nitrous oxide isotopes were purchased from Icon Services Inc. The stated isotopic concentrations of 456 and 546 are both 99% in each sample. Photo-ionization mass spectroscopy (PIMS) combined with IR spectroscopy gave the abundances of 97.4% and 97.6% (with about 0.2% uncertainty) for 456 and 546, respectively. PIMS was performed with a time-of-flight mass spectrometer in the photochemistry end-station at the National Synchrotron Radiation Laboratory (NSRL) in Hefei. The absorption spectrum in the 1200–3500 cm^{−1} region was recorded by a Bruker IFS 120HR interferometer with a multi-pass gas cell that had an adjustable path length. The whole interference chamber was evacuated to less than 0.4 mbar to reduce background absorption and interference from atmospheric gases. Because of the wide spectral range and the large variations in absorption band intensities, different experimental conditions were applied for the measurements, as listed in Table 1. The gas sample pressure was measured using two capacitance manometers (MKS Baratron 627B) with 1 and 20 Torr full-scale ranges at 0.15% accuracy. Different optical filters were applied to improve the signal to noise ratio and to allow for high-resolution measurements. The line positions were calibrated using the absorption lines of water and carbon dioxide. Their values were taken from HITRAN

* Corresponding author. Fax: +86 551 3602969.

E-mail address: awliu@mail.ustc.edu.cn (A.W. Liu).

[3]. The accuracy of the unblended and not-very-weak line is estimated to be better than 0.001 cm^{-1} . The spectra we recorded of

456 and 546 enriched samples are presented in the upper and lower panels of Fig. 1, respectively.

Table 1
Experimental conditions of $^{14}\text{N}^{15}\text{N}^{16}\text{O}$ and $^{15}\text{N}^{14}\text{N}^{16}\text{O}$ nitrous oxide.

Detector	Pressure (Pa)	Path length (M)	Temperature (K)	Range (cm^{-1})	Resolution (cm^{-1})	Isotopic species
InSb	779	105	284	3300–4300	0.01	456
InSb	779	15	286	3300–4300	0.01	456
InSb	148	15	286	3300–4300	0.01	456
InSb	779	105	286	2550–3250	0.006	456
InSb	779	15	288	2550–3250	0.006	456
InSb	779	15	286	2000–2400	0.006	456
InSb	779	15	289	1700–2100	0.006	456
MCT	779	15	289	1250–1650	0.005	456
InSb	1507	87	298	3300–4300	0.01	546
InSb	1507	15	300	3300–4300	0.008	546
InSb	507	15	300	3300–4300	0.008	546
InSb	118	15	299	3300–4300	0.008	546
InSb	28	15	297	3300–4300	0.008	546
InSb	1507	87	299	2550–3250	0.008	546
InSb	1507	15	299	2550–3250	0.008	546
InSb	507	15	297	2550–3250	0.008	546
InSb	118	15	298	2550–3250	0.008	546
InSb	28	15	296	2550–3250	0.008	546
InSb	507	15	299	2000–2400	0.006	546
InSb	118	15	299	2000–2400	0.006	546
InSb	28	15	296	2000–2400	0.006	546
InSb	507	15	300	1700–2100	0.006	546
InSb	114	15	297	1700–2100	0.005	546
MCT	507	15	299	1250–1650	0.005	546
MCT	114	15	296	1250–1650	0.005	546

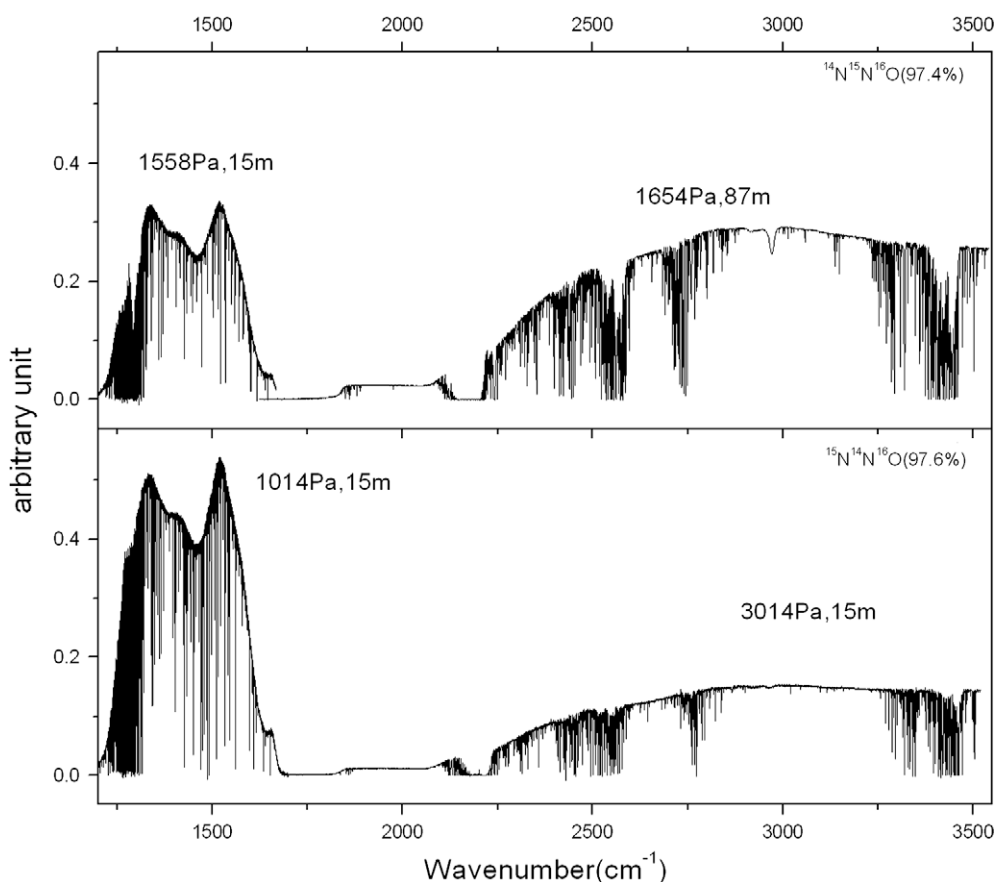


Fig. 1. The Fourier-transform absorption spectrum in the $1200\text{--}3500\text{ cm}^{-1}$ region. Upper panel: N_2O -456 enriched sample. Lower panel: N_2O -546 enriched sample.

3. Rovibrational analysis

3.1. Vibrational assignment

The observed transitions have been assigned using the effective Hamiltonian developed by Teffo et al. [4,5]. Preliminary sets of effective Hamiltonian parameters for 456 and 546 were obtained by Vlasova et al. [6]. The effective Hamiltonian we adopted is based on a polyad structure that results from the approximate relations between the harmonic frequencies $\omega_3 \approx 2\omega_1 \approx 4\omega_2$. Since the mix between the (V_1, V_2^{12}, V_3) states may be strong, the vibrational energy levels are labeled using the triplet ($P = 2V_1 + V_2 + 4V_3, l_2, i$) where the index i increases with energy. In the studied region, all the bands correspond to $\Delta P < 7$ and the spectrum is mostly dominated by hot bands of 456 and 546 species.

The analyzed bands of 456, include 65 parallel ($\Delta l_2 = 0$) bands (34 $\Sigma-\Sigma$, 18 $\Pi-\Pi$, 10 $\Delta-\Delta$, 3 $\Phi-\Phi$), 30 perpendicular ($\Delta l_2 = 1$) bands (12 $\Pi-\Sigma$, 4 $\Pi-\Delta$, 8 $\Sigma-\Pi$, 2 $\Phi-\Delta$, 4 $\Delta-\Pi$), and 3 $\Delta-\Sigma$ ($\Delta l_2 = 2$) cold bands. The bands for the 546 isotopologue are 70 parallel ($\Delta l_2 = 0$) bands (34 $\Sigma-\Sigma$, 19 $\Pi-\Pi$, 12 $\Delta-\Delta$, 4 $\Phi-\Phi$, 1 $\Gamma-\Gamma$), and 28 perpendicular ($\Delta l_2 = 1$) bands (11 $\Pi-\Sigma$, 2 $\Pi-\Delta$, 8 $\Sigma-\Pi$, 2 $\Phi-\Delta$, 5 $\Delta-\Pi$), and 3 $\Delta-\Sigma$ ($\Delta l_2 = 2$) cold bands.

Finally, 7 $\Sigma-\Sigma$ bands and 1 $\Pi-\Pi$ band of the 556 isotopologue, 3 $\Sigma-\Sigma$ cold bands of the 458 isotopologue, 6 $\Sigma-\Sigma$ cold bands of the 548 isotopologue, 1 $\Sigma-\Sigma$ cold band of the 457 isotopologue, and 1 $\Sigma-\Sigma$ cold band of the 547 isotopologue were identified.

Fig. 2 shows the Q-branch of 13^10-02^20 of the 456 isotopologue centered at 1852.28 cm^{-1} . The Q-branch head of the perpendicular hot band 22^20-01^10 of the 546 isotopologue is shown in Fig. 3.

The plot in Fig. 4 compares our newly observed bands (including our two previous works) with those reported by other groups for the 546 isotopologue. The line intensities as provided by the polyad model [6] were adopted for these plots, with the intensity cut-off fixed at $5 \times 10^{-25} \text{ cm/molecule}$.

3.2. Band-by-band rotational analysis

The standard expression below for the vibration–rotation energy levels was used to determine the spectroscopic parameters:

$$F_v(J) = G_v + B_v J(J+1) - D_v J^2(J+1)^2 + H_v J^3(J+1)^3, \quad (1)$$

In (1), G is the vibrational term value, B_v is the rotational constant, and D_v and H_v are centrifugal distortion constants. The spectroscopic parameters for an upper state were fitted directly to the observed line positions of the respective band, and in the case of a hot band involving e and f rotational levels, the ee , ef , fe , and ff sub bands were considered independently. The lower state rotational constants were constrained to their literature values. The observed line positions together with the residuals are given in Supplementary Materials (I). The spectroscopic parameters of 108 newly observed bands for 456, 546 and 458–548 isotopologues, respectively are listed in Tables 2–4. The 110 previously reported bands [7–11] are given in Supplementary Materials (II); our work looked at transitions of higher J value and gave more accurate spectroscopic constants, which were reviewed and given in Supplementary Materials (II). Since some upper vibrational states have been reported in other bands, the corresponding bands and references are also indicated in Supplementary Materials (II) for completeness. The RMS values of the (observed–calculated) deviations are mostly less than $1.0 \times 10^{-3} \text{ cm}^{-1}$, which is consistent with the experimental accuracy of the line positions. It is worth noting that 16 of the bands of the 456 and 546 isotopologues were found rising from (03^10) , (03^30) , (04^20) and (04^40) lower states with high angular quantum number. Though the four lower states were not reported previously, the observed transitions allowed us to obtain the spectroscopic constants of these lower states. The difference between the upper and lower vibrational term values were determined, which are listed together with B_v and D_v in Tables 2 and 3. Notice that the vibrational term value for the (03^30) state of the 546 isotopologue could be

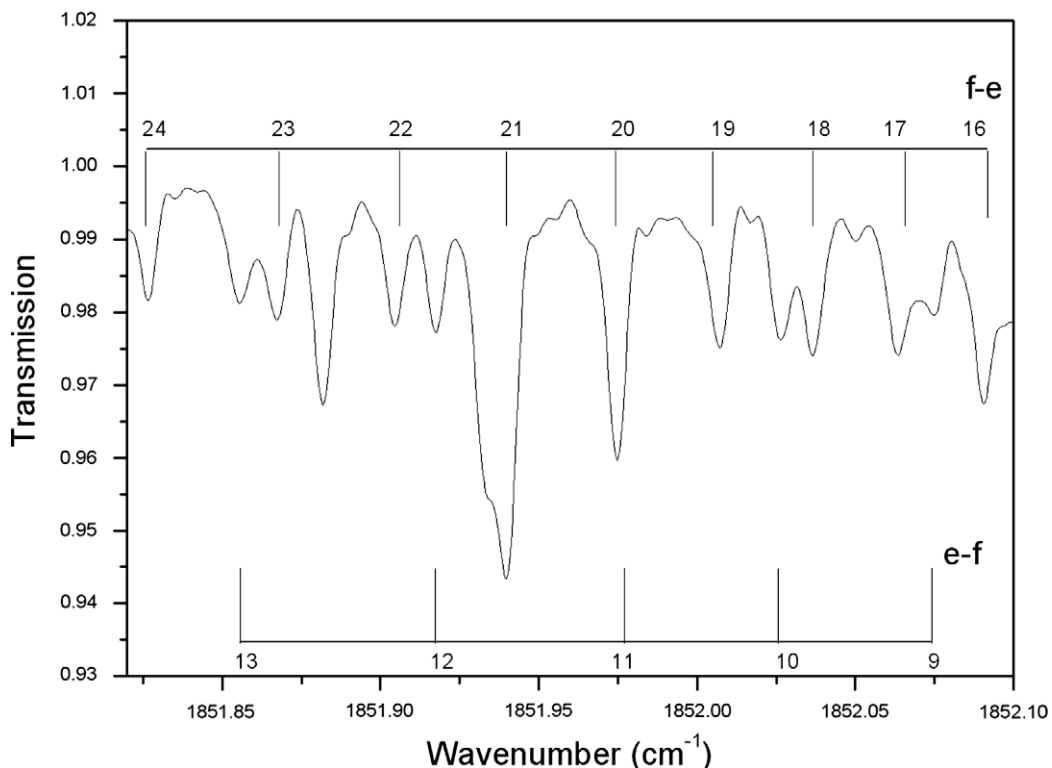


Fig. 2. The Q-branch of the 13^10-02^20 $\Pi-\Delta$ hot band of $\text{N}_2\text{O}-456$ at 1852.28 cm^{-1} and the rotational assignments are presented. The spectrum was recorded at a pressure of 779 Pa and equivalent path length of 15 m.

indirectly derived from the (13^30-02^20) and (03^30-02^20) bands to be 1756.5769 cm^{-1} .

4. Discussion and conclusion

In the last three decades, the 456 and 546 isotopologues have been studied in the $1200-3500\text{ cm}^{-1}$ region by Amiot [9] and Toth

[7,8,10] using enriched isotopic and natural abundance samples, respectively. The ΔG_v deviation of Amiot's work from that of Toth's work is plotted in Fig. 5 for the 456 and 546 isotopologues. It is obvious that the line positions of Amiot's work need to be recalibrated. Figs. 6 and 7 show the ΔG_v deviations of our work from that of Amiot's and Toth's respectively, as a function of wavenumber. It is clear that our results are consistent within the experimental

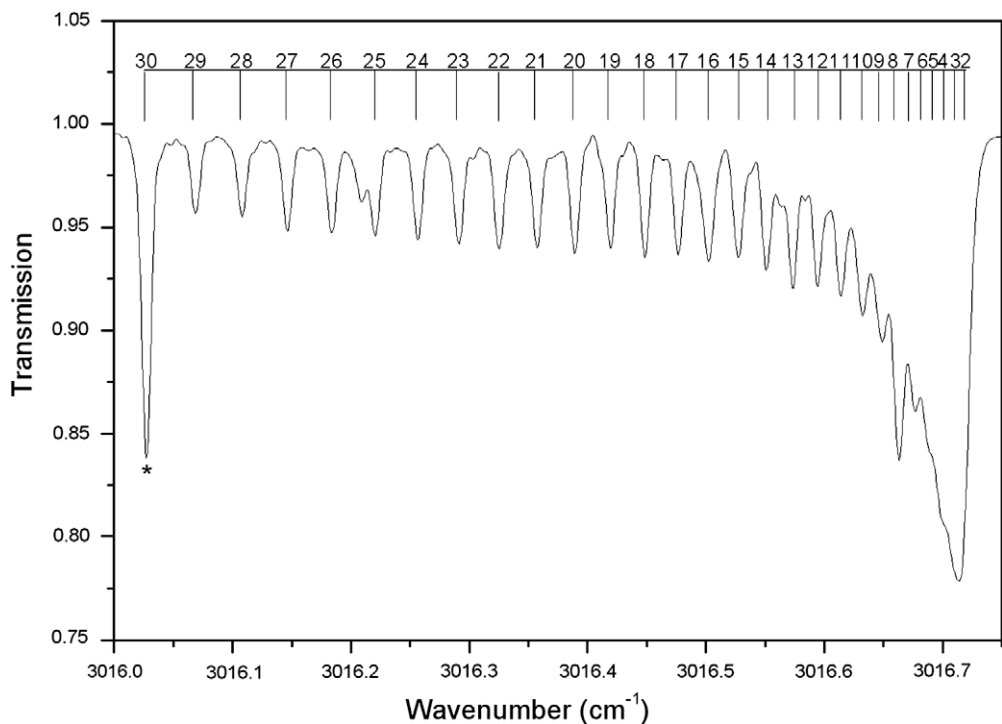


Fig. 3. The Q-branch of the 22^20-01^10 Δ -II hot band of N_2O -546 at 3016.72 cm^{-1} and the rotational assignments are presented. The spectrum was recorded at a pressure of 1507 Pa and equivalent path length of 87 m. The line marked with “*” is blended with the P(5) transition of the 21^10-00^00 band of N_2O -546 molecule at 3020.09 cm^{-1} .

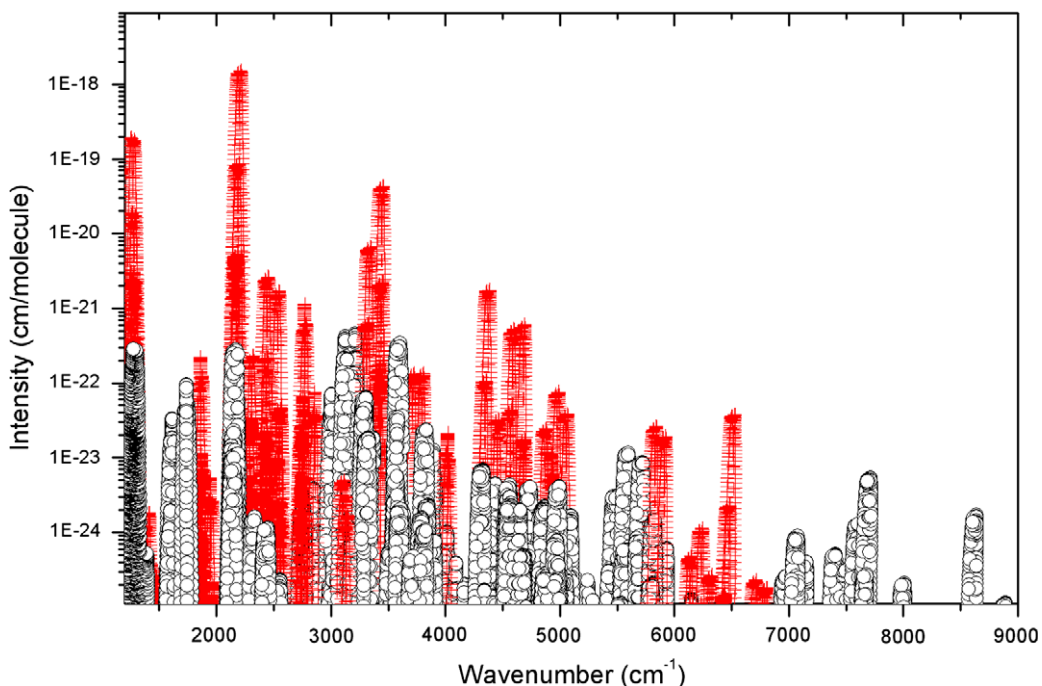


Fig. 4. A list of the transitions assigned for N_2O -546 between 1200 and 9000 cm^{-1} as predicted by the effective Hamiltonian [4,5]. The newly assigned bands and the bands reported in Refs. [7–10] are presented with a circle and a plus, respectively. Note the logarithmic scale adopted for the line intensities.

Table 2

Spectroscopic parameters (in cm^{-1}) of the rovibrational bands of $^{14}\text{N}^{15}\text{N}^{16}\text{O}$ that were assigned in the FTS spectra between 1200 and 3500 cm^{-1} . The cold and hot bands are listed and ordered according to their ΔG_v values.

$V_1 V_2 / V_3$	G_v	B_v	$D_v \times 10^7$	$H_v \times 10^{12}$						
<i>Lower states constants</i>										
$00^0\text{Oe}^{[8]}$	0.0	0.418981810	1.763264							
$01^1\text{Oe}^{[7]}$	575.43365	0.419108916	1.785826							
$01^1\text{Of}^{[7]}$	575.43365	0.419918641	1.794459							
$02^0\text{Oe}^{[8]}$	1144.33338	0.419921722	2.845420	6.6796						
$02^2\text{Oe}^{[8]}$	1151.03090	0.420032300	9.540000							
$02^2\text{Of}^{[8]}$	1151.03090	0.420034800	1.813000							
$10^0\text{Oe}^{[8]}$	1280.35412	0.417127307	1.754555	4.7195						
$11^1\text{Oe}^{[7]}$	1860.19121	0.417273136	1.773906							
$11^1\text{Of}^{[7]}$	1860.19121	0.418165235	1.760323							
$00^0\text{1e}^{[7]}$	2177.65681	0.415654098	1.756773	1.2541						
$04^2\text{Oe}^{[7]}$	2278.19266	0.420684310	5.029130	3.0009						
$04^2\text{Oe}^{[e]}$	2284.35444	0.4207706	-0.848	-31.02						
$12^0\text{Oe}^{[7]}$	2431.32249	0.418090902	2.744112	4.2985						
$12^2\text{Oe}^{[7]}$	2439.59880	0.418286100	1.874700	3.1770						
$12^2\text{Of}^{[7]}$	2439.59910	0.418282900	1.047500	2.4250						
ΔG_v^a	Type	Bands ^b	$(P, \ell_2, i)^c$	G_v						
				B_v						
				$D_v \times 10^7$						
				$H_v \times 10^{12}$						
				Observed lines						
				n/N^d						
				$RMS \times 10^3$						
<i>Cold bands</i>										
2843.35131(24)	$\Pi-\Sigma$	$05^1\text{0e}-00^0\text{0e}$	(5 1 2)	2843.35131(24)	0.4198874(22)	2.973(52)	12.8(34)	P27/R31	32/35	0.38
2843.35135 (48)		$05^1\text{0f}-00^0\text{0e}$		2843.35135 (48)	0.4080645 (27)	3.020 (28)		Q31	17/18	0.95
3301.79976(13)	$\Delta-\Sigma$	$02^2\text{1e}-00^0\text{0e}$	(6 2 1)	3301.79976(13)	0.41677944(29)	0.8073(17)	-6.465(27)	P66/R64	90/97	0.36
<i>Hot bands</i>										
1254.53648(19)	$\Sigma-\Sigma$	$10^0\text{1e}-00^0\text{1e}$	(6 0 3)	3432.19329(19)	0.41379260(62)	1.7480(28)		P38/R48	33/44	0.64
1264.06729(43)	$\Sigma-\Sigma$	$30^0\text{0e}-20^0\text{0e}$	(6 0 6)	3816.47552(43)	0.4135297(39)	1.803(66)		P28/R26	19/25	0.92
1276.78664(15)	$\Pi-\Pi$	$21^1\text{0e}-11^1\text{0e}$	(5 1 4)	3136.97785(15)	0.41546704(28)	1.747(1)		P53/R55	54/63	0.52
1276.78713(14)		$21^1\text{of}-11^1\text{of}$		3136.97834(14)	0.4164663(3)	1.6884(12)		P57/R50	56/65	0.47
1278.48672(57)	$\Sigma-\Sigma$	$14^0\text{0e}-12^0\text{0e}$	(6 0 5)	3709.80921(57)	0.416278(5)	2.9(1)	15.5(57)	P32/R35	23/26	0.91
1280.70595(28)	$\Delta-\Delta$	$22^2\text{0e}-12^2\text{0e}$	(6 2 4)	3720.30505(28)	0.4165721(14)	1.026(13)		P32/R32	38/45	0.73
1280.70567(28)		$22^2\text{of}-12^2\text{of}$		3720.30447(28)	0.4165751(12)	1.747(11)		P32/R34	37/47	0.75
1289.29377(21)	$\Pi-\Pi$	$13^1\text{0e}-03^1\text{0e}$	(5 1 3)	f	0.41765330(32)	2.07550(91)		P61/R59	73/73	0.91
1289.29590(90)		$13^1\text{0e}-03^1\text{0f}$			0.4176708(77)	2.208(92)		Q28	11/11	1.60
1289.2923(19)		$13^1\text{0f}-03^1\text{0e}$			0.4193267(28)			Q32	10/11	2.00
1289.29464(23)		$13^1\text{0f}-03^1\text{0f}$			0.4193474(37)	2.2613(120)		P58/R58	72/72	1.00
1588.56791(25)	$\Pi-\Pi$	$01^1\text{1f}-02^2\text{0e}$	(5 1 1)	2739.59881(25)	0.416613(1)	1.7955(81)		Q36	33/33	0.65
1588.56725(38)		$01^1\text{1f}-02^2\text{0f}$		2739.59815(38)	0.4166205(52)	1.84(12)		P33/R19	16/16	0.65
1595.2642(14)	$\Pi-\Sigma$	$01^1\text{1e}-02^0\text{0e}$	(5 1 1)	2739.5976(14)	0.415832(16)	1.94(34)		P19/R19	9/12	0.96
1595.26465(34)		$01^1\text{1f}-02^0\text{0e}$		2739.59803(34)	0.4166219(21)	1.883(25)		Q29	23/24	0.58
1602.223126(74)	$\Sigma-\Pi$	$00^0\text{1e}-01^1\text{0e}$	(4 0 1)	2177.656776(74)	0.41565397(22)	1.7552(13)		P46/R43	86/88	0.35
1602.223010(57)		$00^0\text{1e}-01^1\text{0f}$		2177.656660(57)	0.41565440(13)	1.76105(55)		Q57	49/50	0.21
1852.28488(73)	$\Pi-\Delta$	$13^1\text{0e}-02^2\text{0e}$	(5 1 3)	3003.31578(73)	0.4176798(64)	2.40(13)		P23/R18	15/19	1.01
1852.28730(42)		$13^1\text{0f}-02^2\text{0e}$		3003.31820(42)	0.4193426(22)	2.261(23)		Q31	21/22	0.79
1852.28782(36)		$13^1\text{0f}-02^2\text{0f}$		3003.31872(36)	0.4193410(29)	2.153(44)		P27/R21	21/25	0.73
1852.28713(37)		$13^1\text{0e}-02^2\text{0f}$		3003.31803(37)	0.4176703(23)	2.157(28)		Q29	21/23	0.79
1856.62456(23)	$\Pi-\Sigma$	$21^1\text{0e}-10^0\text{0e}$	(5 1 4)	3136.97868(23)	0.4154614(17)	1.669(32)	-4.0(16)	P36/R36	50/58	0.60
1856.62426(23)		$21^1\text{0f}-10^0\text{0e}$		3136.97838(23)	0.4164647(12)	1.679(13)		Q32	27/28	0.57
1858.98444(16)	$\Pi-\Sigma$	$13^1\text{0e}-02^0\text{0e}$	(5 1 3)	3003.31782(16)	0.41767010(68)	2.1625(51)		P38/R35	51/57	0.51
1858.98333(32)		$13^1\text{0f}-02^0\text{0e}$		3003.31671(32)	0.4193574(13)	2.4047(92)		Q37	16/18	0.49
1867.62074(22)	$\Phi-\Delta$	$13^3\text{0e}-02^2\text{0e}$	(5 3 2)	3018.65164(22)	0.4188141(15)	1.622(23)	5.5(10)	P41/R34	49/54	0.58
1867.61989(25)		$13^3\text{0f}-02^2\text{0f}$		3018.65079(25)	0.41881487(93)	1.4607(67)		P39/R34	50/55	0.77
1985.94791(36)	$\Pi-\Delta$	$21^1\text{0e}-02^2\text{0e}$	(5 1 4)	3136.97881(36)	0.4154620(26)	1.791(33)		P29/R17	28/29	0.85
1985.94750(35)		$21^1\text{0f}-02^2\text{0e}$		3136.97940(38)	0.4164646(16)	1.746(10)		Q35	32/33	0.92
1985.94765(25)		$21^1\text{0f}-02^2\text{0f}$		3136.97855(25)	0.4164661(15)	1.690(16)		P32/R20	37/43	0.74
1985.94804(35)		$21^1\text{0e}-02^2\text{0f}$		3136.97894(35)	0.4154641(15)	1.733(12)		Q36	31/33	0.90
1992.64286(61)	$\Pi-\Sigma$	$21^1\text{0e}-02^0\text{0e}$	(5 1 4)	3136.97624(61)	0.4154925(68)	2.52(21)	63(17)	P29/R17	19/20	0.60
1992.64377(57)		$21^1\text{0f}-02^0\text{0e}$		3136.97715(57)	0.4164736(26)	1.824(25)		Q30	18/18	0.60
2125.05574(27)	$\Delta-\Delta$	$12^2\text{1e}-12^2\text{0e}$	(8 2 3)	4564.65484(27)	0.4150353(15)	1.085(17)	3.98(49)	P49/R34	36/49	0.70
2125.05581(26)		$12^2\text{1f}-12^2\text{0f}$		4564.65461(26)	0.4150343(13)	1.860(12)	3.32(31)	P53/R46	37/46	0.70
2125.21505(27)	$\Delta-\Delta$	$04^2\text{1e}-04^2\text{0e}$	(8 2 1)	4409.56945(27)	0.417597(1)	-0.8996(95)	-32.94(24)	P53/R30	45/47	0.66
2125.38998(64)	$\Sigma-\Sigma$	$20^0\text{1e}-20^0\text{0e}$	(8 0 5)	4677.79821(64)	0.4119503(24)	1.703(17)		P39/R34	29/34	0.14
2125.44403(25)	$\Sigma-\Sigma$	$12^2\text{1e}-12^0\text{0e}$	(8 0 4)	4556.76652(21)	0.4148403(11)	2.740(13)	4.92(41)	P50/R48	35/44	0.45
2125.53523(34)	$\Sigma-\Sigma$	$04^0\text{1e}-04^0\text{0e}$	(8 0 2)	4403.72789(34)	0.4175140(14)	5.055(13)	31.4(3)	P55/R49	47/60	0.99
2137.47391(60)	$\Phi-\Phi$	$03^3\text{1e}-03^3\text{0e}$	(7 3 1)	f	0.4172728(14)	1.4206(56)		P55/R49	29/29	0.70
2137.47328(48)		$03^3\text{1e}-03^3\text{0f}$			0.417242(12)			Q26	7/8	0.59
2137.47328(48)		$03^3\text{1f}-03^3\text{0e}$			0.4172783(12)			Q25	7/7	0.59
2137.47412(63)		$03^3\text{1f}-03^3\text{0f}$			0.4172347(11)	1.244(34)		P61/R56	31/33	0.75
2138.3806(2)	$\Pi-\Pi$	$11^1\text{1e}-11^1\text{0e}$	(7 1 3)	3998.5719(2)	0.41399058(27)	1.76435(75)		P63/R48	46/47	0.58
2138.38023(25)		$11^1\text{1f}-11^1\text{0f}$		3998.57144(25)	0.4148602(3)	1.75548(76)		P62/R59	44/47	0.53
2148.9600(2)	$\Sigma-\Sigma$	$00^2\text{0e}-00^0\text{1e}$	(8 0 1)	4326.6168(2)	0.41231796(39)	1.7505(15)		P53/R38	37/38	0.53
2258.32316(21)	$\Delta-\Delta$	$06^2\text{0e}-02^2\text{0e}$	(6 2 2)	3409.35406(21)	0.4214023(11)	1.8961(96)		P36/R22	35/41	0.66
2258.32374(19)		$06^2\text{0f}-02^2\text{0f}$		3409.35464(19)	0.42139692(76)	2.7935(54)		P40/R36	51/57	0.67
2288.16474(39)	$\Sigma-\Sigma$	$22^0\text{0e}-10^0\text{0e}$	(6 0 4)	3568.51886(39)	0.4187942(22)	4.481(22)		P24/R29	24/27	0.63

Table 2 (continued)

ΔG_v^a	Type	Bands ^b	(P, ℓ_2 , i) ^c	G_v	B_v	$D_v \times 10^7$	$H_v \times 10^{12}$	Observed lines	n/N ^d	RMS $\times 10^3$
2420.80335(67)	$\Pi-\Pi$	03 ¹ 1e-03 ¹ 0e	(7 1 1)	f	0.4179262(43)	2.964(57)	P29/R24	27/27	1.22	
2420.8027(47)		03 ¹ 1f-03 ¹ 0f			0.4203801(29)	3.136(36)	P31/R26	41/41	1.32	
2421.93971(58)	$\Phi-\Phi$	07 ³ 0e-03 ³ 0e	(7 3 4)	4148.71365 ^g	0.4193967(35)	1.518(43)	P29/R27	37/44	1.18	
2421.94006(56)		07 ³ 0f-03 ³ 0f		4148.71248 ^g	0.4193992(31)	1.562(34)	P30/R28	42/46	1.23	
2423.7679(13)	$\Pi-\Pi$	15 ¹ 0f-11 ¹ 0f	(7 1 5)	4283.9591(13)	0.4175676(93)	2.08(14)	P22/R23	13/14	0.99	
2500.14137(28)	$\Sigma-\Sigma$	20 ⁰ 1e-00 ⁰ 1e	(8 0 5)	4677.79818(28)	0.4119503(16)	1.703(15)	P26/R34	29/33	0.81	
2545.93783(29)	$\Pi-\Pi$	31 ¹ 0e-11 ¹ 0e	(7 1 6)	4406.12904(29)	0.41370878(63)	1.6881(26)	P52/R49	37/53	0.90	
2545.93811(19)		31 ¹ 0f-11 ¹ 0f		4406.12932(25)	0.41485521(46)	1.562(2)	P50/R46	47/53	0.64	
2689.70542(36)	$\Sigma-\Pi$	04 ⁰ 1e-03 ¹ 0e	(8 0 2)	f	0.4174781(19)	4.421(19)	P33/R30	32/35	0.96	
2689.70698(53)		04 ⁰ 1e-03 ¹ 0f			0.4174850(28)	4.478(28)	Q31	16/19	0.83	
2695.54254(64)	$\Delta-\Pi$	04 ² 1e-03 ¹ 0e	(8 2 1)	f	0.4176115(36)	-42.107(46)	P33/R23	24/25	1.29	
2993.08428(15)	$\Sigma-\Pi$	22 ⁰ 0e-01 ¹ 0e	(6 0 4)	3568.51793(15)	0.4188069(13)	4.825(24)	24.2(13)	36/R35	39/41	0.33
2993.08718(51)		22 ⁰ 0e-01 ¹ 0f		3568.52083(51)	0.4187812(19)	4.342(14)	Q38	29/35	0.97	
3014.87784(41)	$\Pi-\Pi$	01 ¹ 2e-11 ¹ 0e	(9 1 1)	4875.06095(41)	0.4125086(42)	1.3(1)	-26.2(71)	P32/R29	48/55	0.86
3014.87446(27)		01 ¹ 2f-11 ¹ 0f		4875.06567(27)	0.4133134(14)	1.790(14)	P32/R30	43/58	0.60	
3134.38057(15)	$\Sigma-\Pi$	22 ⁰ 0e-01 ¹ 0e	(6 0 5)	3709.81422(15)	0.41625729(87)	2.669(11)	3.77(34)	P18/R46	54/54	0.51
3134.38100(25)		22 ⁰ 0e-01 ¹ 0f		3709.81465(25)	0.41625200(83)	2.582(5)	Q41	32/32	0.66	
3139.62552(55)	$\Pi-\Sigma$	15 ¹ 0e-02 ⁰ 0e	(7 1 5)	4283.95890(55)	0.4157635(29)	2.086(34)	P9/R27	12/12	0.56	
3144.87098(22)	$\Delta-\Pi$	22 ⁰ 0e-01 ¹ 0e	(6 2 4)	3720.30463(22)	0.4165719(12)	0.914(15)	-3.69(48)	P34/R45	43/49	0.60
3144.87184(26)		22 ⁰ 0f-01 ¹ 0e		3720.30554(26)	0.41656980(78)	1.7272(43)	Q43	29/38	0.62	
3144.87145(15)		22 ⁰ 0f-01 ¹ 0f		3720.30510(15)	0.41656993(31)	1.7209(12)	P55/R53	44/51	0.50	
3144.86986(36)		22 ⁰ 0e-01 ¹ 0f		3720.30351(36)	0.4165792(11)	1.0177(62)	Q41	31/37	0.78	
3182.28352(13)	$\Sigma-\Sigma$	00 ² 0e-02 ⁰ 0e	(8 0 1)	4326.61690(13)	0.41231878(55)	1.7659(42)	P38/R36	71/71	0.54	
3242.29651(27)	$\Pi-\Pi$	05 ¹ 1e-03 ¹ 0e	(9 1 2)	4956.32056 ^g	0.4167666(84)	2.6384(48)	P44/R43	62/70	0.97	
3242.29451(18)		05 ¹ 1f-03 ¹ 0f		4956.31658 ^g	0.41902860(67)	3.1130(47)	P41/R37	57/62	0.65	
3255.66718(31)	$\Pi-\Pi$	13 ¹ 1e-11 ¹ 0e	(9 1 4)	5115.85839(31)	0.4144869(13)	2.1502(98)	P37/R33	14/24	0.50	
3255.66849(39)		13 ¹ 1f-11 ¹ 0f		5115.85970(39)	0.4161164(22)	2.224(25)	P31/R29	23/35	0.75	
3362.30036(39)	$\Sigma-\Sigma$	30 ⁰ 1e-20 ⁰ 0e	(10 0 8)	5914.70859(39)	0.4101691(12)	1.6172(76)	P41/R39	22/29	0.69	
3377.60659(24)	$\Sigma-\Sigma$	22 ⁰ 1e-12 ⁰ 0e	(10 0 6)	5808.92908(24)	0.4130140(13)	2.634(13)	P32/R32	27/34	0.57	
3377.98784(19)	$\Sigma-\Sigma$	10 ⁰ 2e-00 ⁰ 1e	(10 0 3)	5555.64465(19)	0.41044954(56)	1.734(3)	P46/R43	47/53	0.67	
3388.75653(23)	$\Pi-\Pi$	21 ¹ 1e-11 ¹ 0e	(9 1 5)	5248.94774(23)	0.41218542(48)	1.729(2)	P52/R50	60/75	0.76	
3388.75706(21)		21 ¹ 1f-11 ¹ 0f		5248.94827(21)	0.41315423(43)	1.6765(17)	P55/R50	45/56	0.63	
3401.83418(19)	$\Pi-\Pi$	13 ¹ 1e-03 ¹ 0e	(9 1 4)	5115.85823 ^g	0.41448190(45)	2.1043(20)	P55/R44	53/54	0.74	
3401.83442(19)		13 ¹ 1f-03 ¹ 0f		5115.85649 ^g	0.41611960(42)	2.2576(18)	P52/R49	55/58	0.67	

Notes: The lower state constants and the number that appear between square brackets were set at the values in Refs. [7,8]. The uncertainties given in parenthetically are in unit of the last quoted digit.

^a Difference between the upper and lower vibrational term values.

^b Normal mode labeling according to the maximum value of the modulo of the expansion coefficients of an eigenfunction. In the cases, when there are two candidates for the same labeling or modulo of two principal expansion coefficients practically coincide, we give in parentheses the second variant of the labeling. Note that as a result of strong mixing among the various vibrational modes, the normal mode labeling of some states differs from that given in the previous analysis.

^c Cluster labeling notation: (P = 2V₁ + V₂ + 4V₃, ℓ_2 , i) for the upper state of the band; i is the order number within the cluster that increase with energy.

^d n: Number of transitions included in the fit; N: number of assigned rotational transitions.

^e This work.

^f The vibrational term values are not given due to the indirect rotational constants of the lower vibrational state; they have been determined by other bands.

^g The vibrational term values should be cited with caution because of the indirect rotational constants of the lower vibrational state.

Table 3

Spectroscopic parameters (in cm⁻¹) of the rovibrational bands of ¹⁵N¹⁴N¹⁶O that were assigned in the FTS spectra between 1200 and 3500 cm⁻¹. The cold and hot bands are listed and ordered according to their ΔG_v values.

$V_1 V_2 V_3$	G_v	B_v	$D_v \times 10^7$	$H_v \times 10^{12}$
<i>Lower states constants</i>				
00 ⁰ 0e ^[8]	0	0.404857965	1.642938	
01 ¹ 0e ^[7]	585.31212	0.405037265	1.656798	
01 ¹ 0f ^[7]	585.31212	0.405781109	1.667421	
02 ⁰ 0e ^[7]	1159.97171	0.405712750	2.227530	2.2070
02 ⁰ 0e ^[8]	1170.84300	0.405951200	1.218000	
02 ⁰ 0f ^[8]	1170.84300	0.405950400	1.691000	
10 ⁰ 0e ^[8]	1269.89198	0.403263601	1.597707	3.6343
03 ¹ 0e ^[7]	1736.6478	0.405410775	1.914464	
03 ¹ 0f ^[7]	1736.64792	0.406798997	1.995707	
11 ¹ 0e ^[7]	1862.76708	0.403489655	1.609708	
11 ¹ 0f ^[7]	1862.76708	0.404358647	1.575290	
00 ⁰ 1e ^[7]	2201.60529	0.401497172	1.640337	2.3380
04 ⁰ 0e ^[7]	2305.16257	0.406363987	3.382990	9.8352
04 ⁰ 0e ^e	2314.67872	0.4065328	0.4547	-9.846
12 ⁰ 0e ^[7]	2439.62463	0.404060515	2.177559	1.8634
12 ⁰ 0e ^[7]	2454.60580	0.404529300	1.221000	-2.1000
12 ⁰ 0f ^[7]	2454.60610	0.404528500	1.612800	

Table 3 (continued)

ΔG_v^a	Type	Bands ^b	(P, ℓ_2, i) ^c	G_v	B_v	$D_v \times 10^7$	$H_v \times 10^{12}$	Observed lines	n/N^d	RMS $\times 10^3$
<i>Cold bands</i>										
1736.64797(17)	$\Pi-\Sigma$	03 ¹ 0e-00 ⁰ 0e	(3 1 1)	1736.64797(17)	0.40541103(61)	1.9137(38)		P32/R41	64/65	0.70
1736.64740(24)		03 ¹ 0f-00 ⁰ 0e		1736.64740(24)	0.40680070(76)	2.0110(45)		Q42	40/40	0.73
2875.77232(17)	$\Pi-\Sigma$	05 ¹ 0e-00 ⁰ 0e	(5 1 2)	2875.77232(17)	0.4056722(12)	2.328(19)	2.74(77)	P40/R40	62/73	0.58
2875.77150(15)		05 ¹ 0f-00 ⁰ 0e		2875.77150(15)	0.40769140(44)	2.5093(24)		Q45	35/37	0.46
3344.12023(27)	$\Delta-\Sigma$	02 ² 1e-00 ⁰ 0e	(6 2 1)	3344.12023(27)	0.40266089(52)	1.2101(26)	-2.109(35)	P70/R71	82/96	0.81
<i>Hot bands</i>										
1242.04444(25)	$\Sigma-\Sigma$	10 ⁰ 1e-00 ⁰ 1e	(6 0 3)	3443.64973(25)	0.3998834(17)	1.614(17)		P31/R27	23/29	0.62
1260.91889(23)	$\Sigma-\Sigma$	30 ⁰ e-20 ⁰ 0e	(6 0 6)	3795.45095(23)	0.4006397(17)	1.198(23)		P29/R24	29/34	0.58
1272.5033(4)	$\Sigma-\Sigma$	30 ⁰ e-12 ⁰ 0e	(6 0 5)	3712.1280(4)	0.4023353(19)	2.151(78)		P33/R31	29/34	0.67
1272.81510(23)	$\Pi-\Pi$	21 ¹ 0e-11 ¹ 0e	(5 1 4)	3135.58218(23)	0.40206047(56)	1.5237(26)		P48/R45	65/76	0.76
1272.81531(13)		21 ¹ 0f-11 ¹ 0f		3135.58239(13)	0.40311027(33)	1.4138(16)		P49/R47	67/75	0.57
1279.19886(24)	$\Delta-\Delta$	22 ² 0e-12 ² 0e	(6 2 4)	3733.80466(24)	0.403237(2)	1.236(29)		P18/R25	24/25	0.52
1279.19940(31)		22 ² 0f-12 ² 0f		3733.80550(31)	0.4032278(22)	1.418(24)		P31/R29	32/34	0.78
1283.45007(14)	$\Pi-\Pi$	21 ¹ 0e-03 ¹ 0e	(5 1 3)	3020.09787(14)	0.40372159(34)	1.8963(15)		P45/R50	68/76	0.62
1283.449997(94)		21 ¹ 0f-03 ¹ 0f		3020.097917(94)	0.40522867(23)	1.9604(10)		P48/R48	72/80	0.39
1284.76570(28)	$\Sigma-\Sigma$	22 ⁰ e-04 ⁰ 0e	(60 4)	3589.92827(28)	0.4046425(19)	3.082(22)		P25/R28	25/31	0.63
1287.3564(4)	$\Delta-\Delta$	22 ² 0e-04 ² 0	(6 2 4)	3602.03512(4)	0.4049178(19)	5.83(2.0)		P27/R36	34/36	0.97
1289.14104(12)	$\Phi-\Phi$	13 ³ 0e-03 ³ 0e	(5 3 2)	^f	0.40509840(28)	1.5218(12)		P46/R53	77/78	0.54
1289.14163(42)		13 ³ 0f-03 ³ 0e			0.4050979(17)			Q20	11/11	0.59
1374.560129(84)	$\Sigma-\Sigma$	20 ⁰ e-02 ⁰ 0e	(4 0 4)	2534.531839(84)	0.40181661(47)	1.4940(63)	1.31(22)	P44/R44	80/83	0.32
1601.85872(43)	$\Pi-\Delta$	01 ¹ 1e-02 ⁰ 0e	(5 1 1)	2772.70172(43)	0.4017213(37)	1.692(65)		P23/R21	22/22	0.54
1601.85867(32)		01 ¹ 1f-02 ⁰ 0f		2772.70167(32)	0.4024475(17)	1.659(19)		P31/R23	28/30	0.60
1601.8590(4)		01 ¹ 1e-02 ² 0f		2772.7020(4)	0.4017176(19)	1.657(17)		Q35	33/33	1.15
1601.8588(3)		01 ¹ 1f-02 ² 0e		2772.7018(3)	0.4024484(13)	1.64(1)		Q36	34/34	0.80
1616.2933(65)	$\Sigma-\Pi$	00 ¹ e-01 ¹ 0e	(4 0 1)	2201.605379(65)	0.401496025(17)	1.63048(83)		P49/R44	92/93	0.31
1616.29325(5)		00 ¹ e-01 ¹ 0f		2201.60537(5)	0.4014968(13)	1.63784(12)		Q49	47/49	0.19
1865.68959(17)	$\Pi-\Sigma$	21 ¹ 0e-10 ⁰ 0e	(5 1 4)	3135.58157(17)	0.40206429(79)	1.5591(46)		P35/R30	47/52	0.50
1865.69003(75)		21 ¹ 0f-10 ⁰ 0e		3135.58201(75)	0.4031022(11)	1.4019(33)		Q55	28/28	1.05
2145.35195(19)	$\Gamma-\Gamma$	04 ⁴ 1e-04 ⁴ 0e	(8 4 1)	^h	0.4037957(54)	1.5974(29)		P46/R42	56/56	0.66
2145.35172(23)		04 ⁴ 1f-04 ⁴ 0e			0.4037962(28)	1.647(61)		Q21	9/9	0.32
2145.38585(21)	$\Sigma-\Sigma$	20 ⁰ 1e-20 ⁰ 0e	(8 0 5)	4679.91791(21)	0.39841807(86)	1.4448(68)		P38/R30	27/41	0.50
2145.44446(22)	$\Delta-\Delta$	12 ² 1e-12 ² 0e	(8 2 3)	4600.05026(22)	0.40124145(84)	1.2832(57)		P41/R36	33/44	0.63
2145.44545(3)		12 ² 1f-12 ² 0f		4600.0515(3)	0.4012315(13)	1.5762(95)		P38/R35	34/41	0.88
2146.04471(33)	$\Sigma-\Sigma$	12 ⁰ 1e-12 ⁰ 0e	(8 0 4)	4585.66934(33)	0.4007665(25)	2.254(44)	6.2(21)	P39/R35	36/43	0.75
2146.52806(16)	$\Delta-\Delta$	04 ² 1e-04 ² 0e	(8 2 1)	4461.20679(16)	0.4033273(65)	0.6535(44)		P42/R39	36/51	0.52
2146.52862(43)		04 ² 1f-04 ² 0f			0.4033634(12)	2.0936(64)		P49/R43	54/61	1.67
2146.95456(13)	$\Sigma-\Sigma$	04 ² 1e-04 ² 0e	(8 0 2)	4452.11713(13)	0.40314559(71)	3.3836(89)	10.11(29)	P47/R44	51/58	0.41
2159.26336(16)	$\Phi-\Phi$	03 ³ 1e-03 ³ 0e	(7 3 1)	3915.84025 ^g	0.4032340(31)	1.5556(11)		P57/R54	84/84	0.73
2159.26332(15)		03 ³ 1e-03 ³ 0f		3915.84021 ^g	0.4032335(78)	1.5693(71)		Q33	18/18	0.32
2159.26344(44)		03 ³ 1f-03 ³ 0e		3915.83925 ^g	0.4032369(22)	1.596(21)		Q33	21/21	0.98
2159.263529(83)		03 ³ 1f-03 ³ 0f		3915.83934 ^g	0.40323180(16)	1.55009(53)		P58/R56	89/91	0.40
2159.52253(11)	$\Pi-\Pi$	11 ¹ 1e-11 ¹ 0e	(7 1 3)	4022.28961(11)	0.40016362(45)	1.6116(42)	0.5(1)	P54/R50	75/84	0.39
2159.522494(97)		11 ¹ 1f-11 ¹ 0f		4022.289574(97)	0.40100882(49)	1.5881(59)	1.172(19)	P48/R46	66/78	0.31
2172.0013(2)	$\Sigma-\Sigma$	00 ² e-00 ¹ 0e	(8 0 1)	4373.6066(2)	0.39812897(38)	1.6239(12)		P59/R47	55/55	0.74
2320.03609(17)	$\Sigma-\Sigma$	22 ⁰ 0e-10 ⁰ 0e	(6 0 4)	3589.92807(17)	0.4046471(11)	3.189(18)	5.94(73)	P42/R39	62/72	0.54
2428.16718(69)	$\Phi-\Phi$	23 ³ 0e-03 ³ 0e	(7 3 3)	4184.74407 ^g	0.4054503(50)	1.674(98)		P28/R18	32/33	1.31
2433.95306(41)	$\Pi-\Pi$	31 ¹ 0e-11 ¹ 0e	(7 1 5)	4296.72014(41)	0.4020226(11)	1.8471(52)		P28/R43	29/29	0.70
2433.95111(54)		31 ¹ 0f-11 ¹ 0f		4296.71819(54)	0.4036706(15)	1.9124(83)		P34/R41	27/30	0.71
2542.07127(13)	$\Pi-\Pi$	23 ⁰ e-11 ¹ 0e	(7 1 6)	4404.83835(13)	0.40079345(58)	1.4072(61)	0.64(16)	P36/R50	49/53	0.38
2542.07181(16)		23 ¹ 0f-11 ¹ 0f		4404.83889(16)	0.40210251(69)	1.1875(72)	0.6(2)	P52/R55	59/64	0.48
2635.478843(77)	$\Sigma-\Sigma$	30 ⁰ e-02 ⁰ 0e	(6 0 6)	3795.450553(77)	&0.40064212(39)	1.2451(45)	2.28(14)	P49/R47	89/90	0.32
2715.46914(35)	$\Sigma-\Pi$	04 ¹ e-03 ¹ 0e	(8 0 2)	4452.11694(35)	0.4031433(17)	3.351(24)	8.9(9)	P43/R39	45/57	0.65
2715.47027(36)		04 ¹ e-03 ¹ 0f		4452.11819(36)	0.4031336(21)	3.176(24)		Q29	18/20	0.61
2724.5575(6)	$\Delta-\Pi$	04 ² 1e-03 ¹ 0e	(8 2 1)	4461.2053(6)	0.4033270(29)	0.636(29)		P32/R28	21/29	1.00
2724.55904(75)		04 ² 1f-03 ¹ 0e		4461.20689(75)	0.4033202(18)	1.9755(86)		Q44	10/14	0.96
2724.55817(35)		04 ² 1f-03 ¹ 0f		4461.20609(35)	0.403323(2)	1.996(19)		P33/R30	29/37	0.85
2724.5674(19)		04 ² 1e-03 ¹ 0f		4461.2154(19)	0.403229(14)	-1.24(22)		Q27	5/11	1.50
2752.39743(13)	$\Pi-\Sigma$	11 ¹ 1e-10 ⁰ 0e	(7 1 3)	4022.28941(13)	0.40016325(35)	1.6000(16)		P49/P47	56/63	0.49
2752.39781(22)		11 ¹ 1f-10 ⁰ 0e		4022.2898(22)	0.40100780(77)	1.5745(49)		Q40	29/33	0.58
2851.446462(23)	$\Pi-\Delta$	11 ¹ 1e-02 ⁰ 0e	(7 1 3)	4022.28942(23)	0.4001592(11)	1.5(1)		P34/R32	38/44	0.62
2851.44611(38)		11 ¹ 1f-02 ⁰ 0e		4022.28911(38)	0.4010043(16)	1.511(14)		Q34	21/23	0.69
2851.44628(27)		11 ¹ 1f-02 ⁰ 0f		4022.28928(27)	0.4010042(14)	1.470(13)		P34/R31	37/44	0.75
2851.44569(61)		11 ¹ 1e-02 ⁰ 0f		4022.28869(61)	0.4001636(22)	1.619(14)		Q39	18/21	1.25
2862.31768(23)	$\Pi-\Sigma$	11 ¹ 1e-02 ⁰ 0e	(7 1 3)	4022.28939(23)	0.400164(1)	1.6069(87)		P34/R34	33/38	0.55
2862.31835(37)		11 ¹ 1f-02 ⁰ 0e		4022.29006(37)	0.4010048(33)	1.59(5)		Q31	17/19	0.85
3004.61592(11)	$\Sigma-\Pi$	22 ⁰ e-01 ¹ 0e	(6 0 4)	3589.92804(11)	0.40464842(48)	3.224(5)	7.70(13)	P31/R51	71/75	0.42
3004.61715(27)		22 ⁰ e-01 ¹ 0f		3589.92927(27)	0.40463710(83)	3.0381(49)		Q42	37/39	0.77
3016.72239(15)	$\Delta-\Pi$	22 ⁰ e-01 ¹ 0e	(6 2 3)	3602.03451(15)	0.40494233(75)	0.599(9)	-7.93(29)	P28/R46	60/65	0.46
3016.72258(15)		22 ⁰ f-01 ¹ 0f		3602.03470(15)	0.40494344(37)	1.9277(15)		P28/R49	58/63	0.51
3016.72007(49)		22 ⁰ e-01 ¹ 0f		3602.03219(49)	0.4049596(13)	0.8347(69)		Q47	36/40	1.23
3067.75146(17)	$\Pi-\Pi$	01 ² e-11 ¹ 0e	(9 1 1)	4930.51854(17)	0.39839337(49)	1.6437(26)		P46/R46	71/82	0.77
3067.75086(17)		01 ² f-11 ¹ 0f		4930.51794(17)	0.3991108(5)	1.6583(27)		P45/R43	73/81	0.70
3126.81701(24)	$\Sigma-\Pi$	30 ⁰ e-01 ¹ 0e	(6 0 5)	3712.12913(24)	0.4023329(13)	2.153(15)	2.02(47)	P15		

Table 3 (continued)

ΔG_v^a	Type	Bands ^b	(P, ℓ_2 , i) ^c	G_v	B_v	$D_v \times 10^7$	$H_v \times 10^{12}$	Observed lines	n/N ^d	RMS $\times 10^3$
3148.49408(13)	$\Delta-\Pi$	22^20e-01^10e	(6 2 4)	3733.80620(13)	0.40323297(58)	1.2301(54)	-2.28(13)	P23/R52	57/58	0.44
3148.49421(39)		22^20f-01^10e		3733.80633(39)	0.4039763(11)	1.5131(55)		Q46	38/39	1.19
3148.4945(1)		22^20f-01^10f		3733.8066(1)	0.40323179(25)	1.494(1)		P13/R51	53/56	0.40
3148.49345(38)		22^20e-01^10f		3733.80557(38)	0.40323820(11)	1.3003(57)		Q44	39/40	1.11
3213.634547(93)	$\Sigma-\Sigma$	00^20e-02^00e	(8 0 1)	4373.606257(93)	0.39812985(21)	1.62627(84)		P55/R49	96/101	0.48
3253.97492(47)	$\Delta-\Delta$	06^21e-04^20e	(10 2 2)	5568.65364(47)	0.4038941(33)	-0.545(37)		P25/R29	19/27	0.99
3253.97567(70)		06^21f-04^20f	^h		0.4038917(44)	2.400(53)		P26/R31	35/36	1.81
3270.12857(20)	$\Phi-\Phi$	05^31e-03^30e	(9 3 1)	5026.70546 ^g	0.4037998(76)	1.4785(57)		P42/R34	56/57	0.73
3272.9031(2)	$\Pi-\Pi$	05^11e-03^10e	(9 1 2)	5009.5509(2)	0.40251974(87)	2.3471(94)	3.15(27)	P50/R48	67/77	0.62
3272.90316(15)		05^11f-03^10f		5009.55108(15)	0.40448496(37)	2.4936(17)		P50/R48	67/80	0.60
3289.76515(37)	$\Pi-\Pi$	05^11e-11^10e	(9 1 4)	5152.53223(37)	0.4004778(13)	1.8552(98)		P37/R36	38/49	0.85
3289.76442(21)		05^11f-11^10f		5152.53150(21)	0.40194580(82)	1.949(6)		P39/R37	41/57	0.56
3290.36234(19)	$\Delta-\Delta$	04^21e-02^20e	(8 2 1)	4461.20534(19)	0.40331888(57)	0.4591(42)	-7.62(8)	P63/R48	84/97	0.79
3290.36294(39)		04^21f-02^20e		4461.20594(39)	0.4033224(24)	1.975(24)		Q31	17/22	0.90
3290.36309(17)		04^21f-02^20f		4461.20609(17)	0.40331998(54)	1.984(4)	0.378(78)	P63/R54	88/101	0.71
3290.36284(63)		04^21e-02^20f		4461.20584(63)	0.4033071(87)	0.29(17)		Q28	11/16	1.15
3292.14528(12)	$\Sigma-\Sigma$	04^20e-02^00e	(8 0 2)	4452.11699(12)	4452.11699(34)	3.3894(24)	10.370(43)	P65/R59	109/113	0.55
3315.77746(22)	$\Sigma-\Sigma$	12^01e-10^00e	(8 0 4)	4585.66944(22)	0.40076479(77)	2.2043(58)	2.78(11)	P58/R60	68/85	0.89
3377.4153(4)	$\Sigma-\Sigma$	30^01e-20^00e	(10 0 8)	5911.9474(4)	0.3972425(34)	1.090(57)		P25/R23	18/22	0.66
3386.25577(14)	$\Sigma-\Sigma$	10^02e-00^01e	(10 0 3)	5587.86106(14)	0.39649695(46)	1.5764(24)		P43/R44	37/44	0.42
3403.9466(4)	$\Pi-\Pi$	21^11e-11^10e	(9 1 5)	5266.7137(4)	0.3987432(16)	1.554(15)	1.16(36)	R49/P55	48/59	0.12
3403.95000(25)		21^11f-11^10f		5266.71708(25)	0.39974831(53)	1.3830(22)		P52/R49	49/56	0.78
3415.88374(19)	$\Pi-\Pi$	05^11e-03^10e	(9 1 4)	5152.53154(19)	0.40048192(34)	1.891(1)		P61/R45	54/66	0.71
3577.38330(10)	$\Pi-\Pi$	07^10e-01^10e	(7 1 4)	4162.69542(10)	0.40388193(31)	2.293(2)	2.273(33)	P66/R62	97/97	0.47
3577.38249(10)		07^10f-01^10f		4162.69461(10)	0.40603098(17)	2.45298(50)		P64/R60	99/101	0.54

Notes: The lower state constants and those appear between square brackets were set at the values in Refs. [7,8]. The uncertainties given parenthetically are in unit of the last quoted digit.

^a Difference between the upper and lower vibrational term values.

^b Normal mode labeling according to the maximum value of the modulo of the expansion coefficients of an eigenfunction. In the cases, when there are two candidates for the same labeling or modulo of two principal expansion coefficients practically coincide, we give in parentheses the second variant of the labeling. Note that as a result of strong mixing among the various vibrational modes, the normal mode labeling of some states differs from that given in the previous analysis.

^c Cluster labeling notation: ($P = 2V_1 + V_2 + 4V_3, \ell_2, i$) for the upper state of the band; i is the order number within the cluster that increase with energy.

^d n: Number of transitions included in the fit; N: number of assigned rotational transitions.

^e This work.

^f The vibrational term values are not given due to the indirect rotational constants of the lower vibrational state; they have been determined by other bands.

^g The vibrational term values should be cited with caution because of the indirect rotational constants of the lower vibrational state.

^h The vibrational term values are not given due to the absent of vibrational term value of the lower vibrational state.

Table 4

Spectroscopic parameters (in cm^{-1}) of the rovibrational bands of $^{14}\text{N}^{15}\text{N}^{18}\text{O}$ and $^{15}\text{N}^{14}\text{N}^{18}\text{O}$ that were assigned in the FTS spectra between 1200 and 3500 cm^{-1} . The newly observed bands are ordered according to their ΔG_v values.

Isotopologue	$V_1V_2V_3$	G_v	B_v	$D_v \times 10^7$	$H_v \times 10^{12}$					
<i>Lower states constants</i>										
458	00 ⁰ 0e ^[8]	0.0	0.395467600	1.584000						
548	00 ⁰ 0e ^[8]	0.0	0.381919400	1.467000						
ΔG_v^a										
ΔG_v^a	Type	Bands ^b	(P, ℓ_2 , i) ^c	G_v	B_v	$D_v \times 10^7$	$H_v \times 10^{12}$	Observed lines	n/N ^d	RMS $\times 10^3$
458										
1232.869477(57)	$\Sigma-\Sigma$	10^00e-00^00e	(2 0 2)	1232.869477(57)	0.38063669(21)	1.3629(15)	0.390(29)	P30/R61	80/81	0.27
2388.428950(58)	$\Sigma-\Sigma$	12^00e-00^00e	(4 0 3)	2388.428950(58)	0.38094421(23)	1.8598(21)	0.756(50)	P56/R51	102/106	0.27
2465.03136(12)	$\Sigma-\Sigma$	20^00e-00^00e	(4 0 4)	2465.03136(12)	0.37970420(50)	1.1168(50)	1.07(13)	P54/R50	90/92	0.51
3312.83049(12)	$\Sigma-\Sigma$	02^01e-00^00e	(6 0 1)	3312.83049(12)	0.37944735(45)	1.8662(40)	0.749(90)	P58/R53	78/83	0.47
3398.36367(23)	$\Sigma-\Sigma$	10^01e-00^00e	(6 0 3)	3398.36367(23)	0.3774923(28)	1.824(73)	52.2(51)	P42/R40	56/72	0.76
548										
2381.206039(54)	$\Sigma-\Sigma$	12^00e-00^00e	(4 0 3)	2381.206039(54)	0.39462031(23)	2.1697(21)	1.940(54)	P55/R48	89/93	0.24
3277.748605(88)	$\Sigma-\Sigma$	02^01e-00^00e	(6 0 1)	3277.748605(88)	0.3932355(50)	2.2165(65)	2.05(23)	P46/R43	71/73	0.33
3385.190861(61)	$\Sigma-\Sigma$	10^01e-00^00e	(6 0 3)	3385.190861(61)	0.39069769(20)	1.5473(15)	0.276(29)	P59/R60	103/106	0.28

Notes: The uncertainties given parenthetically are in unit of the last quoted digit.

^a Difference between the upper and lower vibrational term values.

^b Normal mode labeling according to the maximum value of the modulo of the expansion coefficients of an eigenfunction. In the cases, when there are two candidates for the same labeling or modulo of two principal expansion coefficients practically coincide, we give in parentheses the second variant of the labeling. Note that as a result of strong mixing among various vibrational modes, the normal mode labeling of some states differs from that given in the previous analysis.

^c Cluster labeling notation: ($P = 2V_1 + V_2 + 4V_3, \ell_2, i$) for the upper state of the band; i is the order number within the cluster that increase with energy.

^d n: Number of transitions included in the fit; N: number of assigned rotational transitions.

uncertainty ($1 \times 10^{-3} \text{ cm}^{-1}$) with those of Toth for both isotopologues. After recalibrating the Amiot's data with the Toth's data, the ΔG_v deviations between our work and Amiot's for 15% of the bands are still beyond the experimental uncertainty. The 456 band

11^10e-01^10e (centered at 3423.1379 cm^{-1}) and the 546 band 14^00e-02^00e (centered at 2279.39769 cm^{-1}) had the largest deviations. The ΔG_v value of the 456 band 11^10e-01^10e determined with our experimental values has a good agreement with that of Toth's

work. It is hard to indicate the reason for this large difference of Amiot's values. Since there are no other data available on the 546 band $14^0\text{Oe} - 02^0\text{Oe}$, its spectroscopic constants are determined from our and Amiot's measurements. A possible reason for why these deviations are so large is in the fitting of the line positions,

where the RMS value of Amiot's work is $3.8 \times 10^{-3} \text{ cm}^{-1}$, three times larger than our experimental uncertainties.

The difference between the line positions of the 456 and 546 isotopologues in the $1200\text{--}3500 \text{ cm}^{-1}$ region and their values predicted by the effective rovibrational Hamiltonian [6] are plotted in

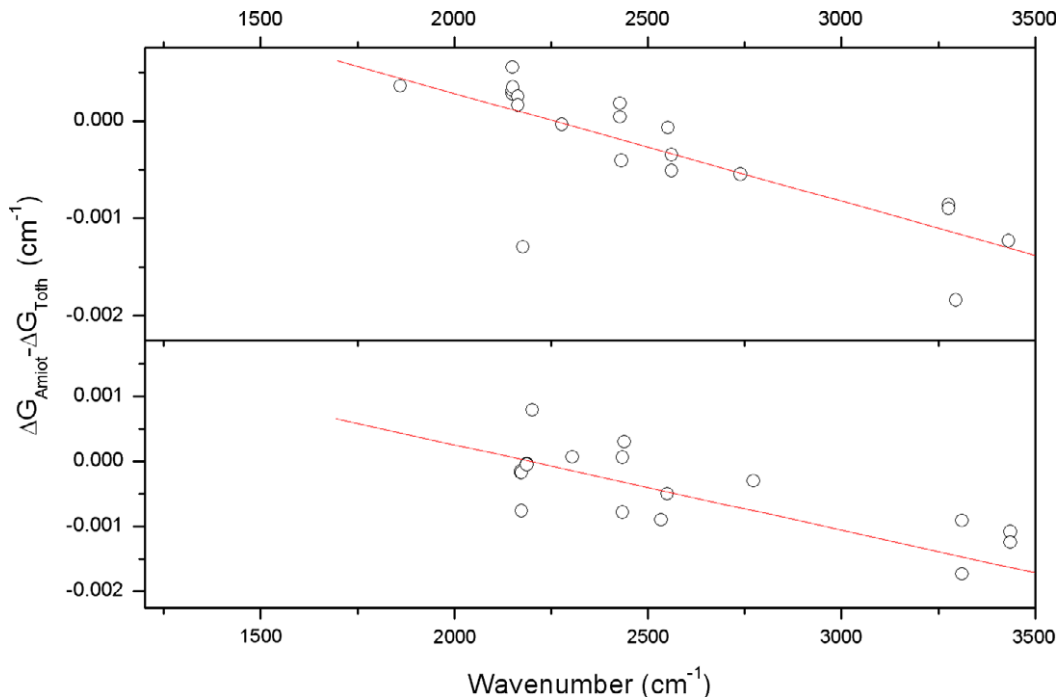


Fig. 5. The differences in the upper and lower vibrational term values (ΔG_v) given by Toth [7,8,10] and Amiot [9] are shown. Upper panel: N₂O-456; lower panel: N₂O-546.

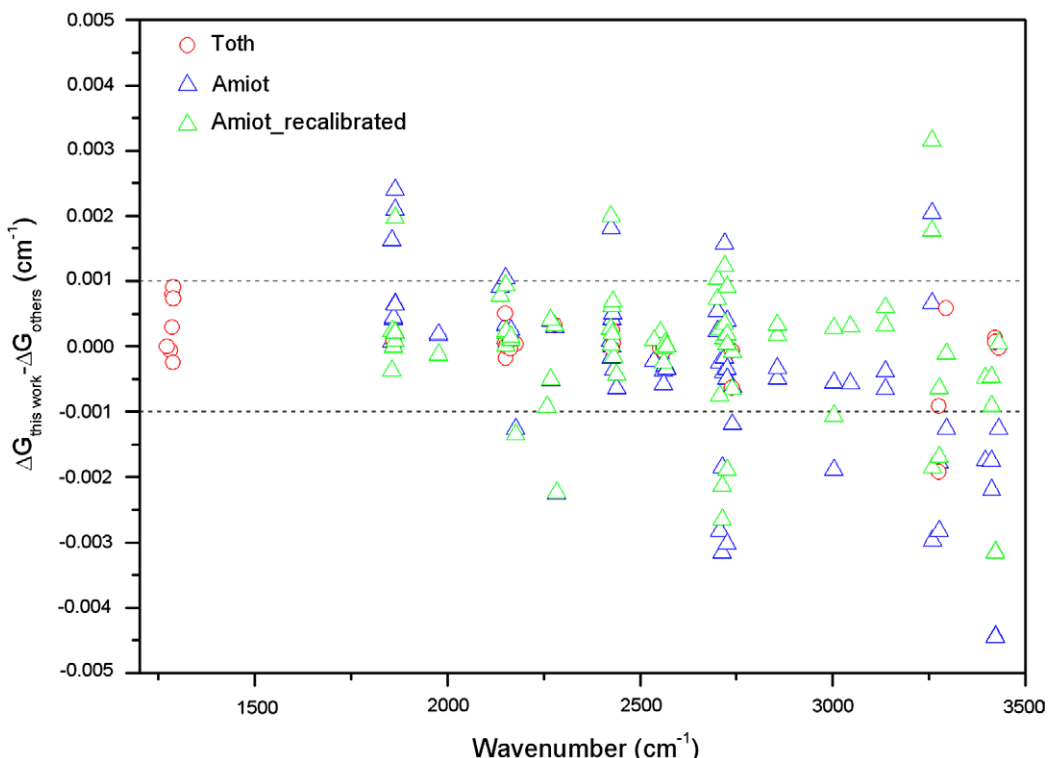


Fig. 6. A plot comparing the difference in the upper and lower vibrational term values (ΔG_v) of N₂O-456 given by Toth [7,8,10], Amiot [9] and this work.

the upper and lower panels of Fig. 8, respectively. The predictive ability of the effective Hamiltonian model is good for both isotopologues since the majority of the residuals lie between -0.01 and 0.01 cm^{-1} .

The present work considerably extends our knowledge about the high-resolution spectra of the 456 and 546 isotopologues of nitrous oxide molecule: 108 new bands have been observed for the first time, and the rotational analysis of other 110 bands has been

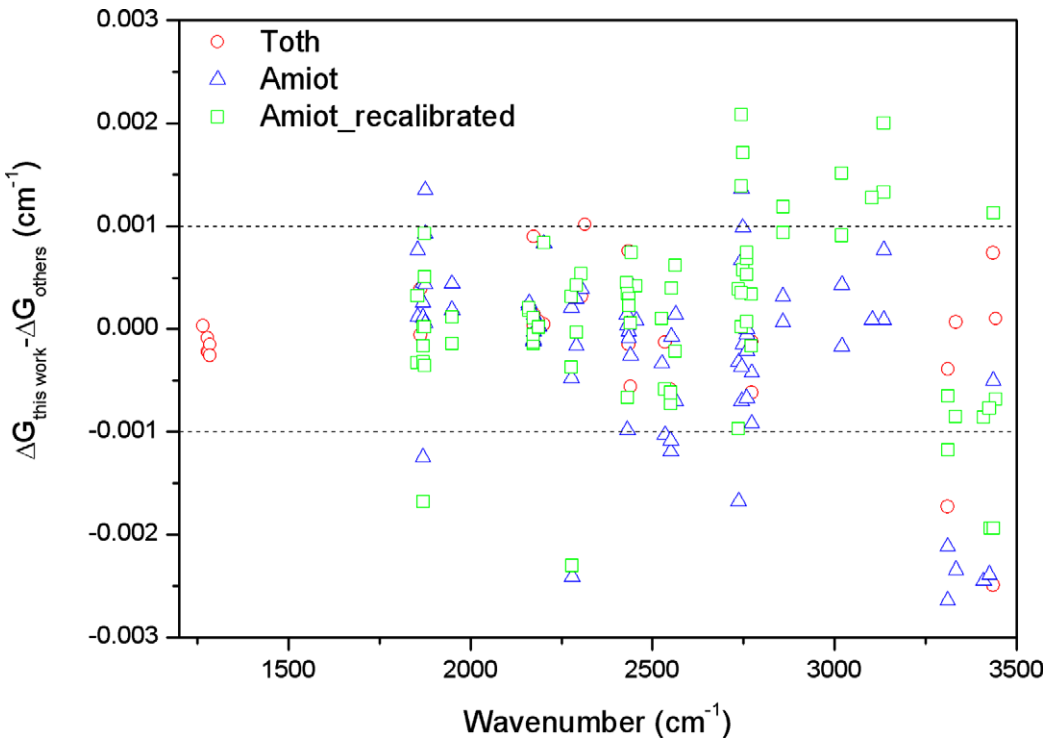


Fig. 7. A plot comparing the difference in the upper and lower vibrational term values (ΔG_v) of $\text{N}_2\text{O}-546$ given by Toth [7,8,10], Amiot [9] and this work.

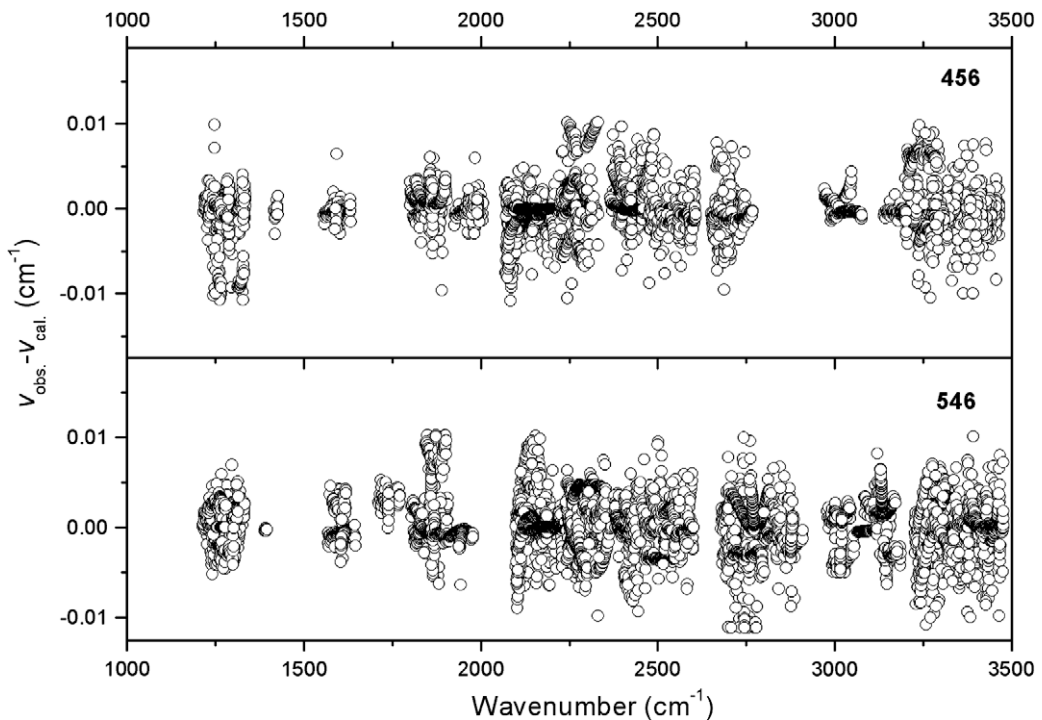


Fig. 8. Difference between the line positions of the $^{14}\text{N}^{15}\text{N}^{16}\text{O}$ and $^{15}\text{N}^{14}\text{N}^{16}\text{O}$ isotopologues of nitrous oxide assigned in the FTS spectrum in the 1200 – 3500 cm^{-1} region and their values predicted by the effective rovibrational Hamiltonian [6].

significantly extended and improved. The polyad model of effective Hamiltonian works well for the majority of the observed bands of 456 and 546 isotopologues except three bands which resonance interactions have not been included in the model.

Acknowledgments

This work is jointly supported by NSFC-China (Grant Nos. 20873132 and 10574124) and RFBR-Russia (Grant No. 06-05-39016), by the Ministry of Science and Technology of China (2007CB815203) and by the Fok Ying Tong Education Foundation (101013). Dr. F. Qi in NSRL (Hefei) is acknowledged for the PIMS mass spectroscopy measurements.

Appendix A. Supplementary data

Supplementary data associated with this article can be found, in the online version, at [doi:10.1016/j.jms.2009.06.012](https://doi.org/10.1016/j.jms.2009.06.012).

References

- [1] H.-Y. Ni, K.-F. Song, V.I. Perevalov, S.A. Tashkun, A.-W. Liu, L. Wang, S.-M. Hu, *J. Mol. Spectrosc.* 247 (2008) 64–75.
- [2] K.-F. Song, A.-W. Liu, H.-Y. Ni, S.-M. Hu, *J. Mol. Spectrosc.* 255 (2009) 24–31.
- [3] L.S. Rothman, D. Jacquemart, A. Barbe, D.C. Benner, M. Birk, L.R. Brown, M.R. Carleer, C. Chackerian Jr., K. Chance, L.H. Coudert, V. Dana, V. Malathy Devi, J.-M. Flaud, R.R. Gamache, A. Goldman, J.-M. Hartmann, K.W. Jucks, A.G. Maki, J.-Y. Mandin, S.T. Massie, J. Orphal, A. Perrin, C.P. Rinsland, M.A.H. Smith, J. Tennyson, R.N. Tolchenov, J. Vander Auwera, P. Varanasi, G. Wagner, *J. Quant. Spectrosc. Radiat. Transfer.* 96 (2005) 139–204.
- [4] J.-L. Teffo, V.I. Perevalov, O.M. Lyulin, *J. Mol. Spectrosc.* 168 (1994) 390–404.
- [5] V.I. Perevalov, S.A. Tashkun, J.-L. Teffo, Sixteenth Colloquium on High Resolution Molecular Spectroscopy, Dijon, France, 6–10 Sept. 1999, Poster D2, p. 103.
- [6] A.V. Vlasova, B.V. Perevalov, S.A. Tashkun, V.I. Perevalov, Fifteenth Symposium on High Resolution Molecular Spectroscopy, Nizhnii Novgorod, Russia, 18–21 July 2006, Poster D20, p. 86.
- [7] R. Toth, *J. Mol. Spectrosc.* 197 (1999) 158–187.
- [8] R.A. Toth, *J. Opt. Soc. Am. B* 4 (1987) 357–374.
- [9] C. Amiot, *J. Mol. Spectrosc.* 59 (1976) 191–208.
- [10] R.A. Toth, *Appl. Opt.* 32 (1993) 7326–7365.
- [11] C. Amiot, *J. Mol. Spectrosc.* 59 (1976) 380–395.